ADVANCED MATERIALS TECHNOLOGIES
www.advmattechnol.de

Strategies to Realize AC Electrokinetic Enhanced Mass-Transfer in Silicon Based Photonic Biosensors.

Anders Henriksson, Peter Neubauer, and Mario Birkholz*

Silicon-on-insulator (SOI) based photonic sensors, particularly those utilizing Photonic Integrated Circuit (PIC) technology, have emerged as promising candidates for miniaturized bioanalytical devices. These sensors offer real-time responses, occupy minimal space, possess high sensitivity, and facilitate label-free detection. However, like many biosensors, they face challenges when detecting analytes at exceedingly low concentrations due to limitations in mass transport. An intriguing method to enhance mass transfer in microfluidic biosensors is AC electrokinetics. Proof-of-concept experiments have demonstrated significant enhancements in limit of detection (LOD) and response times. AC electrokinetics, compatible with silicon photonic sensors, offers techniques such as electroosmosis, electrothermal effects, and dielectrophoresis to modify fluid flow and manipulate particle trajections. This article delves into various approaches for integrating AC electrokinetics into silicon photonic biosensors, shedding light on both its advantages and limitations.

1. Introduction

In biotechnology, regardless of whether applications in early-stage medical diagnosis, environmental monitoring, or optimization of bioprocesses, biosensors are crucial to detect and monitor the appearance and concentration of various biological and chemical substances of interest.

Accordingly, the last decades we have seen the development of a large variety of electrochemical,[1] MEMS-based,[2,3] and optical sensors[4] that now allows the detection of analytes as low as picomolar and even attomolar concentrations.[5] Furthermore, the systems are getting smaller and more user friendly with all necessary functions ideally integrated into single chips, so called Lab-on-a-chip.[6] A technology particularly suitable for miniaturized sensors is silicon-on-insulator (SOI) based photonic sensors.[7–10] SOI based photonic sensors are compatible with well-known standardized semiconductor fabrication processes that allows miniaturization and mass production. In addition, photonic integrated circuit technology (PIC) provides the opportunity for the monolithic integration of electronic and photonic devices, allowing the integration of optical sensors, electrodes, detectors, light-sources, and read-out electronics in a single chip.[11] SOI-based photonic sensors are built based on waveguides allowing the propagation of light and are generally realized as interferometers, often in the form of a Mach–Zehnder interferometer or resonators, often in the form of microring resonators. The sensors allow for real time responses, a minimal footprint, and a high sensitivity. Moreover, it is a label free technique, allowing detection without using signal molecules such as fluorescent or redox markers.[7]

Photonic biosensors as most biosensor approaches generally rely on some form of receptor molecule that is immobilized onto the sensor surface by established silicon surface functionalization protocols.[12–14] The receptor specifically and selectively recognizes a target analyte whose binding is transduced to an electric signal that is further processed and yields information about the bioparticles captured and their concentration. They have been shown to be highly sensitive for detecting biomolecules and sensors in the form of ring resonators have allowed single molecule detection as well as the detection of analytes at concentrations as low as in the femtomolar range. These photonic sensors however, face limitations similar to other sensors at these low concentrations of the desired analytes as it becomes increasingly difficult to transport a small number of molecules in solution to the sensor surface, which can be a major factor in reaching the limit of detection in a reasonable time.[15,16]

The primary means of mass transfer for biomolecular analytes is diffusion or Brownian motion. The size and shape of the analytes, as well as the temperature, dictate the distance they can diffuse in the minutes-to-hours timescale relevant for rapid biomolecular detection, typically ranging from 10 to 100 μm for large biological molecules. This diffusion process is crucial for the analytes to interact with the sensing surface.

Furthermore, as the analyte interacts with the receptor on the sensor surface, the concentration of analytes near the surface is depleted, forming a depletion region. Without convection, the

A. Henriksson, P. Neubauer
Chair of Bioprocess Engineering, Department of Biotechnology
Technische Universität Berlin
Ackerstraße 76, 13355 Berlin, Germany
E-mail: henriksson@campus.tu-berlin.de
M. Birkholz
IHP—Leibniz-Institut für Innovative Mikroelektronik
Im Technologiepark 25, 15236 Frankfurt (Oder), Germany

The ORCID identification number(s) for the author(s) of this article can be found under https://doi.org/10.1002/admt.202302191

DOI: 10.1002/admt.202302191

depletion region will grow over time as more analytes bind to the surface, following longer distances for the diffusion process.[17] For efficient sensing, biosensors are often integrated into microfluidic systems whose small dimensions reduces the diffusion paths and allows specific convection as well as mixing solutions by active or passive means.

Passive systems[18] rely on the geometry and natural flow features to achieve mixing, while active systems[19] utilize external forces to manipulate the fluid in a manner that cannot be achieved through geometry alone. For instance, electric fields[20] or surface acoustic waves[21] can be applied in active systems to induce fluid flow, resulting in a mixing effect or attracting analytes to the sensor surface through specific interactions.

One particular interesting method to increase mass transfer in microfluidic biosensing systems is AC electrokinetics and its realization in biosensors is a growing field of research.[22–24] Proof of principle experiments in ideal solutions have shown a decrease of the limit of detection by several orders of magnitude and shortened the detection time from hours to minutes.[25] The technique is furthermore highly compatible with silicon photonic sensors as state of the art Photonic Integrated Circuits (PIC) technology allow the integration of micro electrodes with various materials within 1–2 μm distance from the silicon waveguide.[26]

AC electrokinetics may increase the mass transfer by changing the fluid flow by electroosmosis[20] or electrothermal effect[27] or for specific interaction with the particles by dielectrophoresis.[28] While increased mass transfer due to fluid flow may shorten the sensor response time, the specificity of dielectrophoresis also has the potential to improve the LOD and avoid non-specific bonding, due to more specific interaction with the particles.[29]

In this article, we discuss various approaches to integrate AC electrokinetics into silicon photonic biosensors, as well as its advantages and disadvantages. In particular, their ability to be combined with modern methods of semiconductor integration makes them a particularly interesting prospect for biosensor technology.

2. Theory

2.1. AC Electrokinetics

The terminology AC electrokinetics involves various methods for manipulating particles and fluids using alternating electric fields. It includes dielectrophoresis, which can interact with micro- and nano-scale objects or AC electroosmosis, and the AC electrothermal effect, both involving fluid motion.

2.1.1. Electroosmosis

Surfaces of most channel materials used in microfluidics such as glass or various polymers are negatively charged in an electrolyte solution at physiological pH. This negative charge results in an electrostatic attraction between the surfaces and positively charged ions, causing the accumulation of cations at the surface while depleting negatively charged ions. This leads to an inhomogeneous distribution of ions at the interface, a phenomenon known as the electric double layer (EDL). The structure of the EDL can be described by the Gouy-Chapman-Stern model. In this model, the interface consists of a thin layer of ions closely attached to the surface and a diffusion layer of ions that are more loosely attracted and exponentially decay in concentration with distance from the surface.[30]

When an AC or DC electric field is applied to electrodes integrated in the channel, the EDL responds to the field. As a result, the net charge of the EDL is induced to move toward the oppositely charged electrode. Due to viscous coupling, the solvent (typically water) is dragged along with the moving ions. This results in a fluid flow known as electro-osmotic flow.[31,32]

Assuming that the double-layer thickness is much smaller than the dimensions of the microfluidic channel cross-section, the electro-osmotic flow u_{EOF} can be mathematically described as

$$u_{\mathrm{EOF}} = \frac{-\varepsilon \zeta_0 E}{\mu} \tag{1}$$

with ε being the permittivity of the medium, ζ_0 being the zeta potential of the wall of the fluidic cell, E being the applied electric field and μ the dynamic viscosity of the fluid.[32]

The AC electroosmotic effect has been applied in various ways to manipulate fluidic streams within microchannels, leading to the development of micropumps,[34,35] micromixers,[36] and flow controllers.[37]

The ability to alter fluidic streams and induce mixing has found practical applications, particularly in facilitating the transport of biomolecules from bulk solutions to sensor surfaces, as illustrated in **Figure 1a**. The movement of ion charges within the electrical double layer on the electrode surfaces generates a rotational fluid motion. This motion induces microfluidic agitation, enhancing the transport of analytes and preventing the formation of a depletion layer, which typically occurs without fluid motion or with convection via laminar flow.[33] This enhanced transport is crucial for improving the efficiency of reactions and detection processes in microfluidic systems. Accordingly, mass transfer efficiency and reduced detection times for various analytical techniques may be achieved.[23]

Furthermore, when combined with dielectrophoretic forces, AC electroosmotic effects have demonstrated the capability to selectively concentrate analytes onto sensor surfaces, offering promising prospects for localized and enhanced sensing applications.[33,38]

2.1.2. Electrothermal Effect

The electrothermal flows is another important effect that may arise by applying an inhomogeneous AC field and which may influence the fluid flow in microfluidic systems. Temperature gradients ∇T within the liquid as a result of Joule heating may cause local gradients in permittivity, conductivity, density, and viscosity, which produce net forces acting on the fluid (Figure 1b). For instance, conductivity gradients produce free volumetric charges and Coulomb forces, whereas permittivity gradients produce dielectric forces.[27]

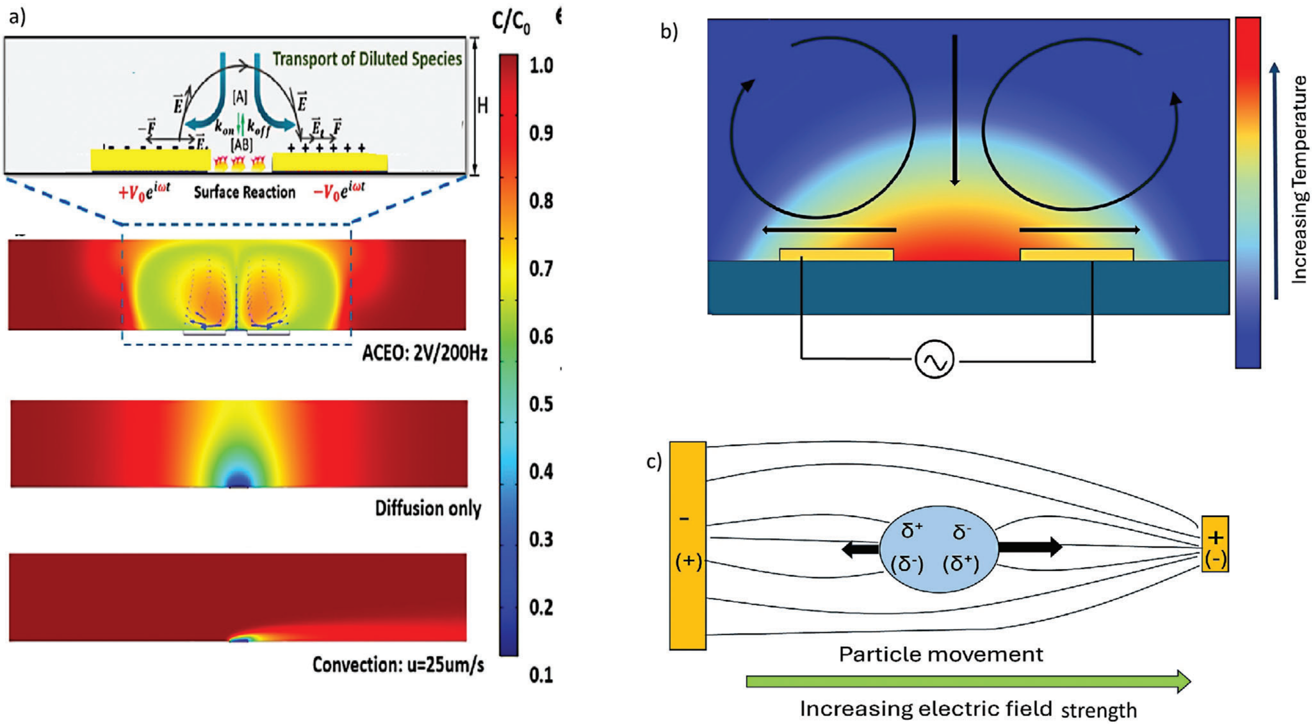

Figure 1. Schematic illustration of AC electrokinetic mechanisms. a) AC Electroosmosis: An applied AC field induces fluid motion from the bulk toward the electrodes, enhancing mixing and preventing the formation of a depletion layer, beneficial for biosensor applications. This effect is simulated and compared to conditions where the analyte is only transported by diffusion or convection. Here, C represents the analyte concentration, and C_0 is the initial analyte concentration. Reproduced with permission.[33] 2017, American Chemical Society. b) Electrothermal effect: Temperature gradients ∇T within the liquid as a result of Joule heating may cause local gradients in permittivity, conductivity, density, and viscosity, which produce net forces acting on the fluid. c) Dielectrophoresis: An applied inhomogeneous electric field generates a force on particles, causing them to move either toward or away from the strongest electric field. If the particles are more polarizable than its immersion medium, they move toward the region of highest electric field strength, a phenomenon known as positive DEP.

The force $\boldsymbol{F_E}$ depends on the frequency f or angular frequency $\omega = 2\pi f$ and can be described as

$$F_{\mathrm{E}} = \frac{1}{2}\frac{\varepsilon(\alpha-\beta)}{1+(\omega t)^2}(\Delta T\cdot E)E + \frac{1}{4}\varepsilon\alpha[E]^2\Delta T \tag{2}$$

where α describes the influence of the temperature on the permittivity and β on the conductivity Assuming a temperature of around 293° K α can be approximated to −0.4% K^{-1} and β to 2% K^{-1} respectively, $\tau = \varepsilon/\sigma$ is the charge relaxation time of the liquid and is in the range of 0.7–35 ns for conductivities in the range of 0.02–1 $S{\cdot}m^{-1}$.

While efficient mixing due to electroosmosis may be applied in medium with low conductivity electro thermal effects are more pronounced in solution with higher ion strength and have the potential to improve biodetection.[31] Some limitations with the approach can be addressed to the local Joule heating generated that may cause degradation or denaturation of the target biomolecules. Other disadvantages are sensitivity to environmental factors such as temperature.

2.1.3. Dielectrophoresis

Dielectrophoresis (DEP) is a phenomenon that occurs when particles are subjected to an oscillating electric field with non-uniform characteristics. This causes a polarizability gradient to arise between the particles and the surrounding medium, based on their respective intrinsic dielectric properties. The induced DEP-force on a spherical particle, with a diameter of d, can be mathematically described as follows:

$$F_{\mathrm{DEP}} = \frac{\pi}{4}d_{\mathrm{p}}^3\cdot\varepsilon_{\mathrm{m}}' Re\left\{\frac{\varepsilon_{\mathrm{p}}^*-\varepsilon_{\mathrm{m}}^*}{\varepsilon_{\mathrm{p}}^*-2\varepsilon_{\mathrm{m}}^*}\right\}\cdot\nabla\left|\vec{E}\right|^2 \tag{3}$$

Here, the Clausius-Mosotti factor plays a crucial role in determining the dielectric properties of the particles (p) and the medium (m). It is expressed as a function of their complex dielectric constants, which in turn depend on the real part of permittivity (ε') and electrical conductivity (σ). These parameters are inherently frequency-dependent, which means that the dielectric properties of the particles and the medium are governed by the frequency (f) or the angular frequency ($\omega = 2\pi f$) at which the voltage is oscillating. Thus, the complex dielectric constants can be expressed as $\varepsilon* = \varepsilon' + i\sigma/\omega$

A crucial characteristic of DEP is its dependency on the real part of the Clausius-Mosotti factor, which can vary between −0.5 to 1.[28] This allows for the DEP force to exhibit either positive (pDEP) or negative (nDEP) values. Positive DEP describes a force that directs particles toward regions with the densest electric field

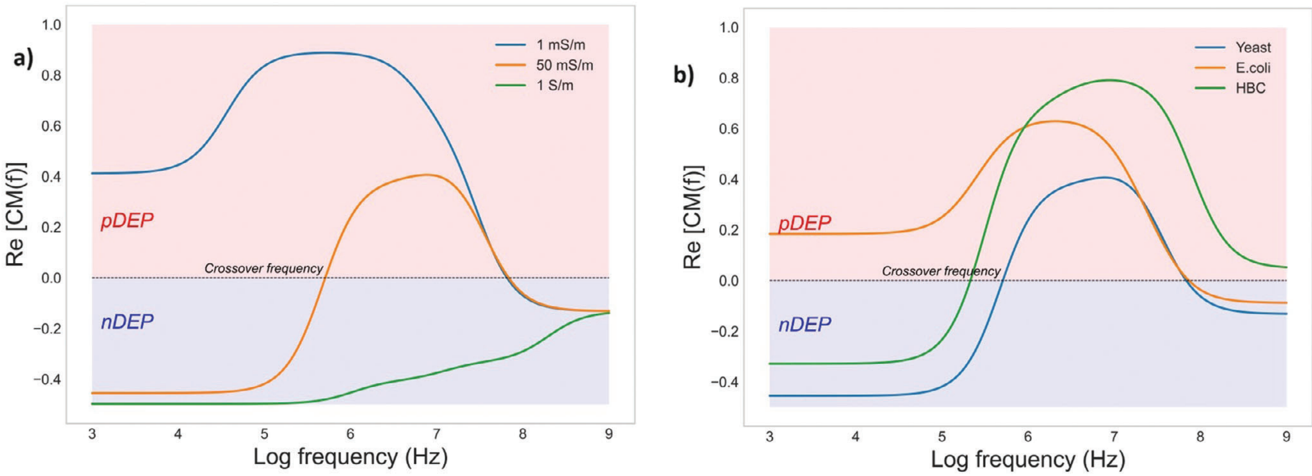

Figure 2. Illustration of the variation of the DEP effect depending on medium conductivity and the dielectric properties of the target microorganism. a) The CM factor as a function of applied frequency f for yeast cells in medium with conductivities of 1, 50, and 1000 mS m^{-1} in the frequency range 1 kHz-1GHz b) The CM factor as a function applied frequency for yeast cells, *Escherichia coli (E. coli)*, and Human B cells (HBC) for a medium conductivity σ_m of 50 mS m^{-1}. Simulations were conducted with the software MyDEP.[47] Reproduced under the terms of the CC-BY 4.0 license.[29]

gradients, whereas negative DEP forces particles away from high-field regions. In terms of frequency dependency, the primary factor determining the dielectrophoretic force (F_{DEP}) transitions from being influenced by electrical conductivity (σ) at lower frequencies to being primarily affected by the real part of permittivity (ε') at higher frequencies.

Another influential parameter affecting particle interaction is the magnitude of the local square of the electric field gradient (∇E^2), which is contingent on the applied voltage (V) and electrode geometry. Consequently, the design of electrodes plays a critical role in shaping the DEP effect. This is particularly significant when manipulating small particles like biomolecules, owing to the cubic relationship between DEP force and particle radius.[22]

DEP has gained interest in biotechnology for separating various microscopic particles, including blood[39] cells, microalgae,[40,41] yeast,[42] viruses,[43] and bacteria.[44] It enables diverse applications such as cell sorting,[45] concentration,[46] and trapping. Additionally, the conductivity of the surrounding medium significantly influences the DEP effect. **Figure 2a** illustrates the simulated CM factor across a frequency range of 10^3-10^8 Hz using a single shell model for Yeast cells (*Saccharomyces cerevisia*) suspended in media with three different conductivities. In low-conductivity media (below 1 mS/m), pDEP occurs at frequencies below 10 MHz, while high-conductivity media (over 100 mS/m) induce nDEP across all frequencies. Moderate-conductivity media exhibit a dynamic DEP response, with a crossover frequency observed—a transition of the CM factor from negative to positive.

For biosensor purposes DEP may thus be applied to push analytes to the sensor surface, thus overcoming limitations due to diffusion and lowering the limit of detection that can be achieved in a reasonable time scale. This approach has proven to be especially effective for enhancing the detection of larger particles in microfluidic systems, such as bacteria. This is because the DEP effect is strong at these dimensions and only a limited number of analytes are present in the sample (e.g. 10^5 colony forming units pro mL) in relevant clinical settings. samples.[24] Furthermore, the larger size of the analytes makes diffusion and Brownian motions negligible, the analytes bind less efficient to the surface and the analysis might be hampered as the cells are actively moving.. Thus, if the cells are not actively brought to the sensor surface, they will just pass in the middle of the channel and not be registered, Accordingly, numerous studies have focused on the use of DEP in various sensing platforms, and it has been demonstrated to improve microbial detection by several orders of magnitude, with detection limits as low as 10^2 CFU mL^{-1}.[44,48] As the DEP effect scales with the cube of particle radius, DEP is less frequently applied to interact with biomolecules such as proteins or oligonucleotides. Nevertheless, also biomolecules can be manipulated[49–52] and the implication of AC electrokinetics enrichment in molecular biosensing has been demonstrated by several research groups using a variety of strategies and shown improvement of the limit of detection by several order of magnitudes as well as reduction in response time.[29]

2.2. Silicon Waveguides and Photonic Integrated Circuits

Photonic integrated circuits can be compared to electronic integrated circuits. However, instead of a current of electrons, photons are transported and instead of using transistors various building blocks such as waveguides and gratings are used to transport, manipulate, and ultimately detect light.

In silicon photonics, silicon is used as the optical medium and a variety of structures and geometries can be used to guide light in the near-infrared wavelengths of ≈1.5 µm. The waveguides are surrounded by a cladding of low refractive index material such as SiO_2 that allows the light to remain in the waveguide and propagate via total internal reflection. Changes in refractive index influences the propagation of the light in the waveguides, which makes them useful for sensor purposes. The fabrication of silicon waveguides involves several crucial steps using Silicon-on-Insulator (SOI) wafers. Initially, photolithography is applied to

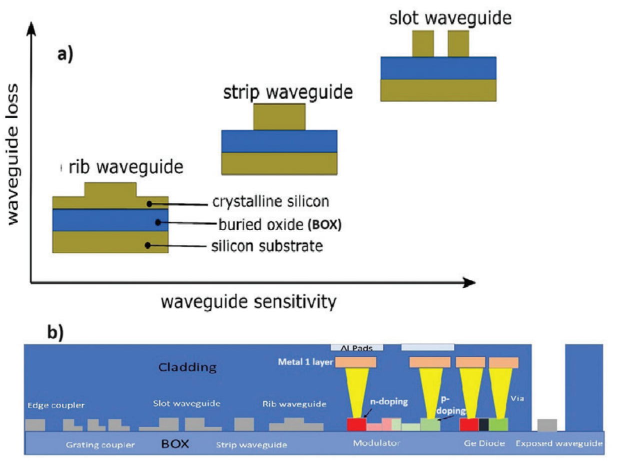

Figure 3. a) Schematic illustration of the sensitivity and optical loss for commonly used waveguides. Reproduced under the terms of the CC-BY 4.0.[7] b) Schematic illustration of commercially available PIC technology.

define the waveguide pattern on the wafer, followed by silicon etching so that only light directing structures remain. To enhance functionalities, additional procedures like doping or component integration can be introduced as needed.

A fraction of the light propagating through the waveguide, known as the evanescent field, extends into the surrounding medium. Consequently, it can interact with the surrounding environment, and even minor changes in its composition can lead to alterations in the effective refractive index. This inherent property allows photonic waveguides to serve as highly sensitive biosensors. In the silicon photonic technology, three types of waveguides are commonly employed, namely rib waveguides, strip waveguides, and slot waveguides (as illustrated in **Figure 3**).

Rib waveguides, with an extended crystalline basis offer the advantage of minimal optical loss during light propagation. However, they exhibit a low sensitivity to environmental changes, such as the binding of analytes.

Slot waveguides, characterized by a gap in waveguide center stand out as the most sensitive waveguide geometry concerning environmental influences. Nevertheless, it's crucial to note that they also suffer from the highest degree of optical loss among these three waveguide types, potentially impacting sensing applications negatively. In this regard, the properties of the strip waveguide are positioned between the rib and the slot waveguide. Consequently, a trade-off exists between optical loss and sensitivity when choosing the waveguide, a dynamic that varies depending on specific application requirements.[7]

2.2.1. Microring Resonator

Microring resonators are simple waveguide-based devices that, in their basic configuration, consist of a looped waveguide adjacent to a straight waveguide. These resonators typically have radii R ranging from 10 to a few 100 µm.. Light is coupled into the straight waveguide through grating couplers, and the intensity of the light propagating through the waveguide is detected by a photodetector.

Under specific resonance conditions, some of the light can couple to the looped waveguide through evanescent field interactions, leading to the observation of narrow dips or valleys in the transmitted light spectrum during a wavelength sweep. These dips in intensity correspond to resonances where the optical energy is temporarily trapped within the ring structure before being coupled back into the straight waveguide.[53,54]

The resonant wavelengths (λr) in microring resonators are typically determined by a harmonic relation to the ring's circumference 2πR.

$$2\pi R n_{\mathrm{eff}} = m\lambda r \tag{4}$$

The effective refractive index (n_{eff}) of a microring resonator is not only dependent on the properties of the waveguide materials but also on the characteristics of the surrounding materials. When organic molecules accumulate on the sensor's surface, they induce a shift in the resonant wavelengths λ_{r} to higher values. This shift is a result of the changes in the effective refractive index n_{eff} caused by the interaction with the deposited molecules.

Furthermore, the effective refractive index is also influenced by the waveguide's geometry. For instance, in strip waveguides, the evanescent field penetrates more deeply into the surrounding materials compared to rib waveguides. Consequently, strip waveguides exhibit higher sensitivity to changes in the surrounding environment. However, as mentioned above, this increased sensitivity comes at the cost of greater optical loss.[7]

2.2.2. Mach-Zehnder Interferometer

The operation of a Mach-Zehnder Interferometer (MZI) in silicon photonic technology is based on the principles of interference, utilizing the interference of light waves to perform various optical functions such as modulation, sensing, and switching.

The MZI begins with a single optical input waveguide that splits into two arms at a waveguide splitter. This splitter effectively divides the incoming optical signal into two separate paths. One of these pathways serves as the reference arm and is typically coated with SiO_2, making it impervious to the surrounding environment. Consequently, the effective refractive index n_{ref} the reference arm remains unchanged, regardless of environmental factors such as changes in gas composition or the presence of electrolyte solutions.

Conversely, the other pathway, known as the sensor arm, is intentionally exposed to the environment. As a result, the refractive index n_s of the sensor arm can vary in response to environmental changes, such as alterations in electrolyte solutions or the binding of analytes to the waveguide's surface.

After traveling through their respective arms, the two waveguides recombine at a Y-coupler, leading to the interference of the two light paths. The resulting interference signal can be expressed as.

$$I_{\mathrm{out}} = I_{\mathrm{R}} + I_{\mathrm{s}} + 2\sqrt{I_{\mathrm{R}} I_{\mathrm{s}} \cos\left(\Delta\varphi + \Delta\varphi_0\right)} \tag{5}$$

where IR and IS are the light intensities of the reference arm and the sensing arm, respectively. $\Delta\varphi_0$ is the initial phase difference between the two arms caused by different effective refractive index due to environment or imperfect waveguide fabrication. φ is the phase difference caused by changes in the sensing solution. Accordingly, analyte interaction with the sensing waveguide changes the effective refractive index of the sensing arm and the changes in the interference pattern can be monitored.[55]

3. Realization of AC Electrokinetics-Enhanced Sensing in Silicon PICs

As reviewed elsewhere,[24] AC electrokinetics has been frequently utilized to enhance microbial detection in various fields. It consistently delivers significant improvements in detection sensitivity, often achieving detection levels as low as 10^2 colony forming units pro mL, representing a substantial leap in performance. Additionally, the detection of biomolecules has also benefited from DEP, resulting in improvements in sensitivity while significantly reducing detection times[29] and even allowing single molecule detection.[56] Furthermore, improvements in packing technologies have allowed advancements toward miniaturized LOC system that can even be wirelessly controlled.[57] Nevertheless, it's crucial to note that, despite these promising advancements, the majority of research in the realm of biomolecule detection using DEP still falls within the domain of proof-of-principle experiments.

There are four common electrode configurations used to create the AC electrokinetics effect in microfluidic setups: The most straightforward electrode configuration consists of a pair of planar electrodes situated opposite each other, often designed with sharp edges to maximize electric field gradients. For efficient AC trapping, interdigitated electrodes (IDE) are commonly employed, allowing for the multiplication of adjacent edges, thus covering a larger area while maintaining a high field gradient. In electrorotation experiments, a quadrupole electrode arrangement, consisting of two pairs of electrodes, is typically used. Furthermore, also 3D electrode configurations, with electrodes positioned in different planes, are frequently employed. In this particular geometry, the electric field is predominantly oriented perpendicular to the substrate, giving preference to dielectrophoresis (DEP) over AC electroosmosis.[22] The key to enabling AC electrokinetics in a photonic biosensor is the successful integration of such electrodes into the PIC.

3.1. PIC Fabrication Technologies

There are currently approximately 20 commercial silicon photonics manufacturing platforms available for prototyping and low volume manufacturing.[58] These platforms are accessible to end-users either in an engineering mode or in a cost-sharing Multi-Project-Wafer (MPW) mode.[11,59] The engineering mode offers the benefit of a customized design, but is more expensive and reserves the entire reticle. The MPW mode, on the other hand, allows users to submit designs for a portion of the reticle, resulting in a few dozen processed chips rather than full wafers, making it a cost-efficient option for low volume chip fabrication. Figure 3 illustrates the most important standard PIC modules available on the most MPW shuttles that are relevant for AC electrokinetic enhanced biosensors. A typical platform allows a variety of waveguides with different geometries and the integration of Ge-diodes[60] and modulators[61] as well as multiple metal layers.[62] An optical modulator is a device that is used to modulate i.e., vary the fundamental -characteristics of a light beam propagating either in free space or in an optical waveguide. The modulators are generally realized by applying doping to the silicon structures thus allowing an electric field to be applied. The silicon layer can be contacted via so called interconnect access (vias) to the metal 1 layers, allowing an applied electric bias and a current flow to modulate the waveguide. For biosensing applications an additional module is required allowing the waveguide to be exposed by selectively etching the cladding SiO_2 at desired positions of the waveguide.

In addition, a wide range of materials are readily accessible through standard PIC fabrication processes. In the Back-End-Of-Line metallization phase, various metals and alloys are frequently employed, including options like Al:Cu, aluminum (Al), copper (Cu), titanium (Ti), titanium nitride (TiN), and tungsten (W). Additionally, a variety of isolators and passivation materials such as silicon dioxide (SiO_2), silicon oxynitride (SiON), and silicon nitride (Si_3N_4) are commonly used.[62] Furthermore, research demonstrations based on heterogeneous integration of new materials include LiNbO3, BaTiO3, PbZrTiO3, organic materials, and 2D materials like graphene.[61]

Integrating new materials or implementing alternative processes within Silicon Photonics frequently encounters several challenges in achieving a seamless and low-loss integration with the Silicon photonic platform. The introduction of defects during integration can significantly diminish the yield of the Photonic Integrated Circuit (PIC) manufacturing process, consequently raising manufacturing costs. As a result, photonic layouts are typically constrained to be compatible with established technologies, i.e., to fit to one of the 20 design kits for which production technologies are available.

3.2. Integrating Electrodes in Silicon Photonics

When integrating electrodes for AC electrokinetics into a PIC, the first metal layer and doped waveguides modules emerge as the most apparent choices that align with standard technology. The metal 1 layer offers a flexible means of electrode placement within the Back-End-Of-Line of the PIC, comprised of low-resistance materials that mitigate side effects like excessive Joule heating. However, a drawback arises from its placement appr. 1–2 µm above the silicon waveguide.[62] This relatively large distance limits the efficacy of AC electrokinetics concentration effects, particularly when employing dielectrophoresis for attracting analytes to the sensing elements. Another concern pertains to the risk of corrosion since metal 1 layers often consist of aluminum or aluminum alloys, which are highly susceptible to corrosion.

For example Birkholz et al,[63] showed that the TiN/Al:Cu/TiN metal-layer stacks that are usually applied in their institute PIC technology[61] cannot be applied as electrodes in aqueous solutions with high concentrations of electrolyte. These layers are comparatively fast subjected to corrosion, which may be understood from small pores and imperfections of the TiN layer via which the electrolyte may corrode the Al:Cu. Also, thin $CoSi_2$ films were found to suffer from changes of their sheet resistance when in contact with buffered saline solutions at elevated temperatures. The effect was however less pronounced than for Al. From a variety of metal layers prepared, only single layers of TiN appeared sufficiently corrosion-resistant and showed only negligible changes of their sheet resistance when in contact with a 90° hot saline solution for a time span of days. Even when polarized in an electrochemical cell between −0.8 and +0.8 V vs. Ag/AgCl, the TiN layer revealed high stability in buffered solution as well as in sulfuric acid. In the presence of redox active species such as hexacyanoferrate or catechol the layers showed no electrocatalytic activity. It can thus be concluded that TiN layers are well suited to serve as CMOS compatible electrodes in bioelectronic devices.

TiN[64] suffers however from a higher resistance ρ of a factor of 2 in comparison to aluminum layers[65] and may generate extensive joule heating.[66] Accordingly, if working in biological solutions the electrode should be prepared by TiN layers while accepting the higher resistivity or a passivation layer that protects the electrodes is required. If the sensors are used at high frequencies and in a low electrolyte concentration the corrosion is less pronounced and may allow standard aluminum materials to be used. Another commercially available option for integrating electrodes onto the chip is to introduce doping, silicide, or other conductive materials into the device layer adjacent to the core waveguide, establishing contact through the metal 1 layers. For this purpose, any kind of standard conductive silicide, such as $TiSi_2$ or $CoSi_2$ can be used.

The demand for highly efficient optical modulators has driven the advancement of such electrically active electrodes positioned in close proximity to the waveguide. These modulators serve as essential components within silicon photonic-based telecommunication systems as they play a pivotal role in encoding information onto optical signals through variations in light intensity (amplitude modulation) or light frequency (frequency modulation).

A modulation may be achieved by applying an electric field to a material in order to change its real and imaginary refractive indices. This change in refractive index (Δn) resulting from an applied electric field is referred to as electro-refraction.[67] The most common method of achieving such modulation in silicon devices so far has been to exploit the plasma dispersion effect, which involves varying the concentration of free carriers through the movement of charge carriers into or out of a waveguide. The three prominent schemes to introduce changes in the free carrier concentration are (a) the injection of minority carriers by forward biasing a PIN junction; (b) the accumulation of majority carriers of opposing polarity across an insulating section in a waveguide; (c) the depletion of majority carriers from a PN junction by reversely biasing it.

Figure 4a illustrates cross-sections of typical device structures that enable such modulation are illustrated. These structures generally comprise selectively doped waveguides connected to the metal 1 layer through interconnect access (vias). By employing alternating n-doped and p-doped regions, it is possible to facilitate the formation of PN junctions on the rib waveguides, allowing modulation through the mentioned mechanisms.

Furthermore, a plethora of variations to achieve optimal junction configurations for a variety of applications has been reported as showcased in Figure 4b. The strategies can be categorized as (i) Vertical P(I)N junction: Here the PN junction is placed horizontally on the top and bottom surfaces of the waveguide, enhancing modulation efficiency and reducing power consumption. (ii) Horizontal or lateral PN junction: Here the PN junction is placed vertically side-by-side in the waveguide center. This design, often modified for better performance: (iii) Interleaved or interdigitated PN junction: This design alternates p-type and n-type doping along the waveguide length, offering good modulation efficiency by balancing speed and power use. The PN junctions may in addition be realized by combining the strategies mentioned above such as the zig-zag phase shifter configuration.[61]

Furthermore, the integration of novel material systems with silicon photonics platforms has demonstrated remarkable modulator performance, all while retaining the advantages offered by the well-established silicon photonic technology, as indicated by recent research findings. These materials can typically be categorized into several groups, including (silicon-)germanium, ferroelectrics, III–V semiconductors, 2D materials, and organic (electro-optic) materials.[61] Early results involving the combination of electro-optic materials with silicon photonic platforms have displayed significant potential for fast modulation.[68]

Another widely employed approach for achieving modulation is through the use of thermo-optic phase shifters, making use of the temperature dependance of the refractive index n. These phase shifters have gained popularity due to their straightforward fabrication process, efficient phase shift modulation, and broad bandwidth capabilities.[69] The operational principle of a thermo-optic phase shifter involves altering the refractive index of both the waveguide n_{wg} and cladding materials n_{clad} by applying current to a resistive heater running alongside them. This change in refractive index dn/dT effectively modifies the optical mode's effective refractive index n_{eff}. Figure 4c illustrates a commonly used configurations for implementing a thermo-optic phase shifter. In one common setup, a silicon waveguide is realized on the device layer, and a heater is positioned above the waveguide on the metal 1 layer. It is worth noting that maintaining a sufficient vertical gap between the heater and the waveguide is essential to prevent excessive optical insertion loss.

Figure 4c also presents an alternative approach and technique for minimizing the vertical separation between the heater and the bus waveguide. In this arrangement, the electrodes are positioned alongside the waveguide within the device layer. To effectively address substantial propagation losses, the inclusion of an optically transparent material, such as a 2D material, becomes crucial. A similar approach has also been applied to enable arrays of individually addressable SOI microring resonators for biosensing.[70]

While the strategies mentioned above for integrating electrodes into a PIC primarily aim to facilitate the creation of modulators, similar approaches involving doped waveguides offer a convenient means to fabricate electrodes for AC electrokinetics. In particular, the use of doped waveguides is a convenient way to introduce electrodes close to the core waveguide using standard fabrication. One drawback associated with this method is its relatively high resistivity,[71] resulting in increased Joule heating when compared to pure metals. However, it is worth noting that the doped waveguide can also be coated with various silicide materials to enhance conductivity.[72] Both the doped waveguides

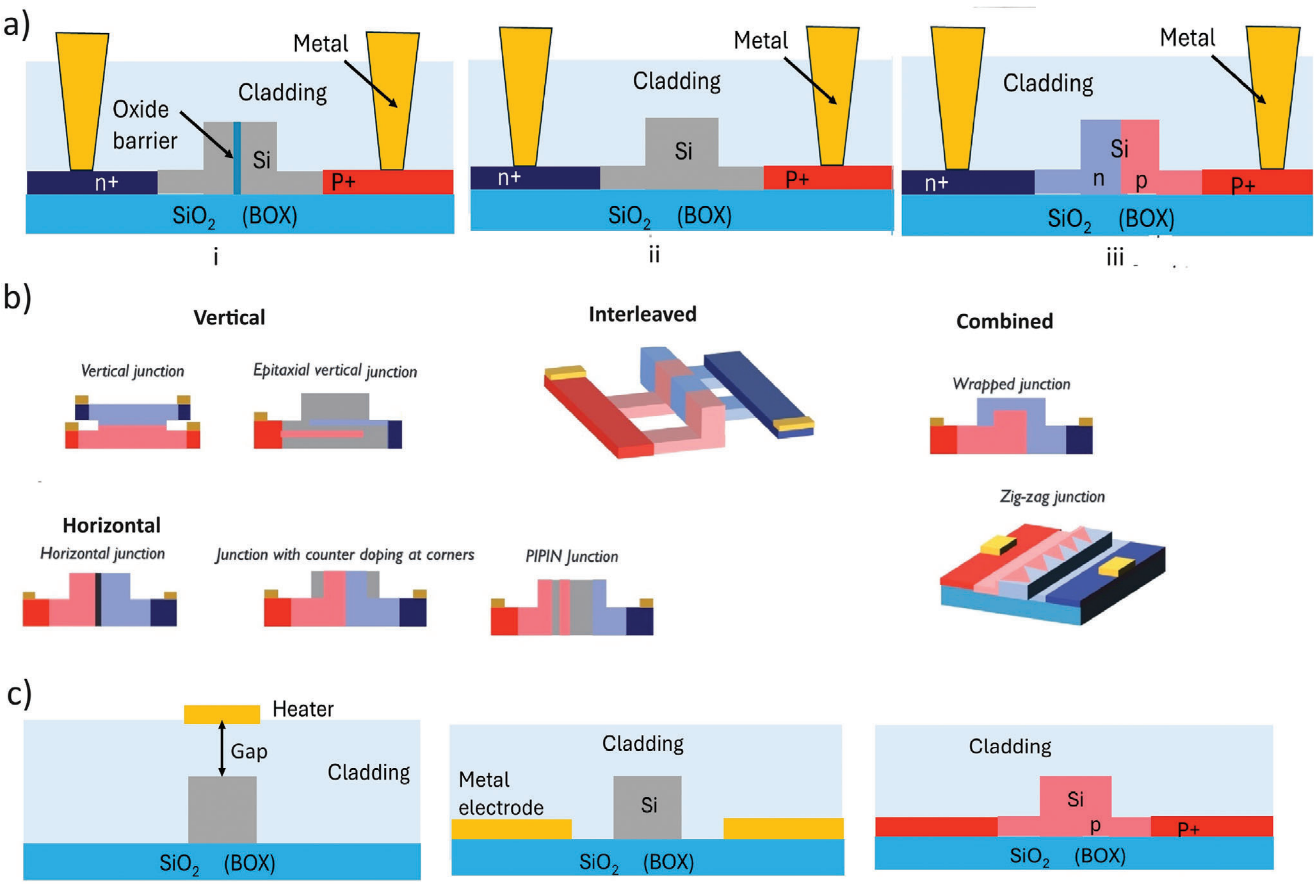

Figure 4. a) Cross-sections of typical device structures implementing the three different mechanisms commonly used to electrically manipulate the free carrier concentrations in plasma-dispersion-based silicon optical modulators: i) Carrier accumulation, ii) Carrier injection; iii) Carrier depletion; Reproduced under the terms of the CC-BY 4.0[67] b) Illustration of the diversity of modulator solutions reported in the literature. Vertical P(I)N junction (vertical junction, epitaxial vertical junction): The PN junction is placed horizontally on the top and bottom surfaces of the waveguide, enhancing modulation efficiency and reducing power consumption. Horizontal or lateral PN junction: The PN junction is vertically side-by-side in the waveguide center. Interleaved or interdigitated PN junction: This design alternates p-type and n-type doping along the waveguide length, offering good modulation efficiency by balancing speed and power use. Combined junction: The junction is realized by a combination of strategies (Zig-Zag junctions, wrapped junction). Reproduced under the terms of the CC-BY 4.0[61] c) Reported solutions to realize thermo-optic phase shifters. A silicon waveguide is etched on the device layer, and a heater is positioned above the waveguide on the metal 1 layer or the electrodes are positioned alongside the waveguide within the device layer.

and these silicide materials exhibit lower corrosiveness compared to aluminum or copper.

3.3. Recent Attempts to Realize AC Electrokinetics in a PIC

There are only a limited number of reports in both journal articles and patent literature where attempts have been made to integrate AC electrokinetics principles into PIC for biosensing applications and these efforts have predominantly focused on the dielectrophoretic effect. One notable example is a 2018 patent application assigned to Fujitsu LTD, (**Figure** 5a) which introduced several innovative approaches to integrate concentration electrodes directly onto the chip.[73]

This patent application demonstrates a carefully integrated design of electrodes into a PIC with the specific goal to precisely guide analyte particles toward the cavity of a slot waveguide. This innovative approach holds significant potential for a wide range of sensor devices, including those reliant on evanescent-field sensing via light scattering, microring resonators, and Mach-Zehnder interferometers.

The rib of the slot waveguide was made conductive through an induced doping process, establishing a connection to the first metal layer. In an especially intriguing variation of the electrode design, the core waveguide itself underwent a doping process, resulting in a thorn-shaped structure. This unique structure has the potential to generate a strong electric field gradient along its edges, enhancing its interaction with analytes and offering interesting possibilities for advanced sensing capabilities.

It is worth noting, however, that their electrode structure bears a striking resemblance to previous approaches used to enable signal modulation through plasma dispersion. While in the case of modulators, the movement of carriers is sought after to modulate the optical signal, this dynamic behavior is less ideal for biosensor applications. Although a modulated signal definitely can be used for biosensing applications,[74] to our opinion a

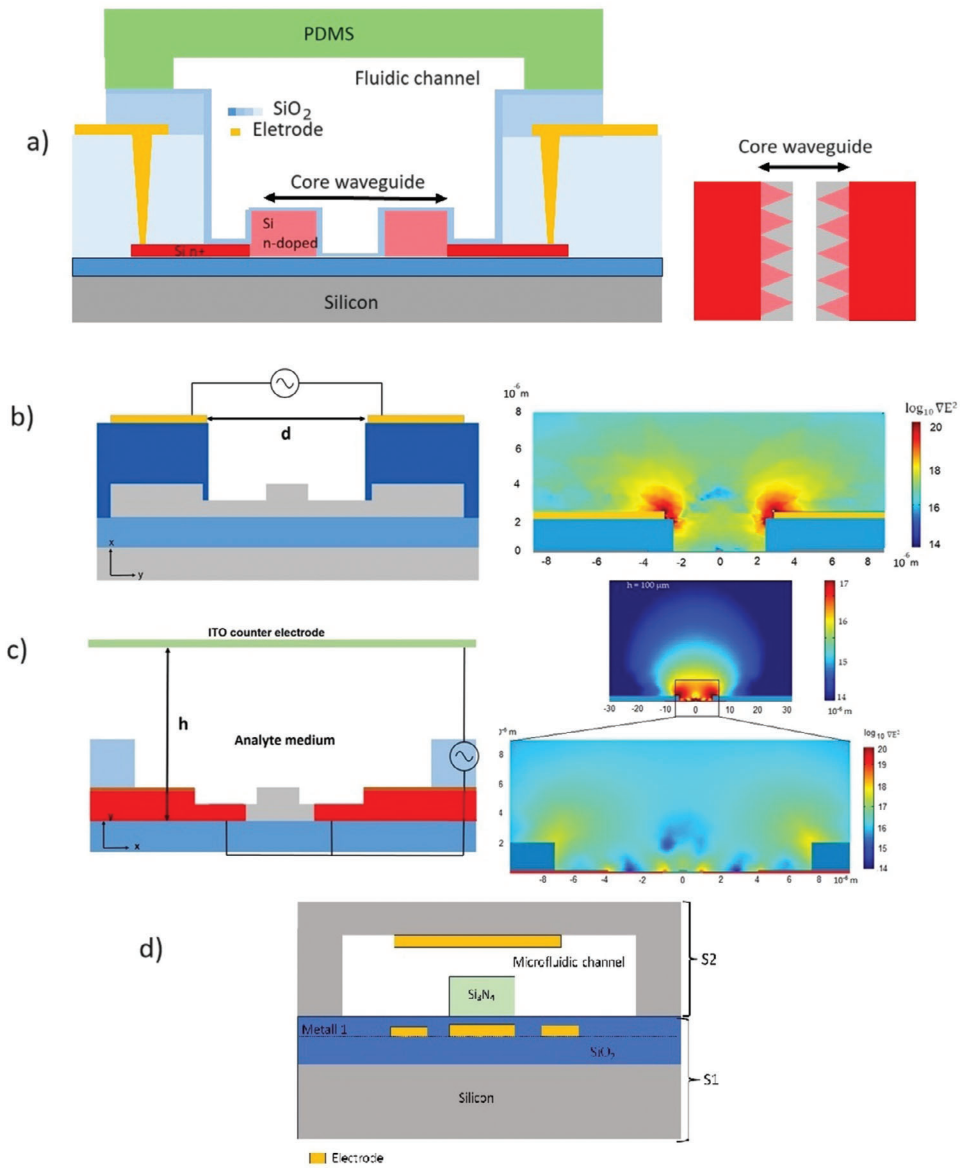

Figure 5. Example of AC electrokinetic biosensor devices. a) A slot waveguide is selectively doped to create electrodes in proximity to the waveguide, facilitating the transport of analytes to the sensor surface. The rib of the slotted waveguide is heavily doped, while a Zigzag structure on the core waveguide, made of moderately doped silicon, is implemented. b) Coplanar electrode pair placed on the metal 1-layer of a SOI-based PIC. Reproduced under the terms of the CC-BY 4.0[26] c) Top bottom electrode configuration. Reproduced under the terms of the CC-BY 4.0[26] d) SiN waveguide with a top-bottom electrode configuration. The waveguide and bottom electrodes are realized by conventional CMOS technology on the substrate S1. A second substrate (S2) is bonded to S1 to realize the microfluidic channel.

sensing response that is independent on the applied AC field would be preferable.

Within our research group, we have previously introduced two distinct electrode configurations aimed at enhancing the sensitivity of a microring resonator through the application of DEP forces.[26] In our first configuration, we positioned electrode pairs on the first metallization layer of the PIC. These electrodes were designed to envelop the exposed waveguide, which forms the sensor's surface. Similar to the work above, thorny-shaped electrode structures were designed to generate high electric fields along their thorn-like edges and ensuring an inhomogeneous distribution of these fields across the electrode gap. Due to constraints inherent to the fabrication process, the angle at the thorn structures was limited to a minimum of 90°.

One significant advantage of this electrode configuration lies in its relatively straightforward implementation. Integrating electrodes onto the first metallization layer can be achieved with relative ease when incorporating them into PIC. However, as mentioned earlier, the available metals and alloys often exhibit corrosive properties, which may necessitate the introduction of a passivation layer to address this issue. A second limitation associated with this configuration pertains to the location of the maximum

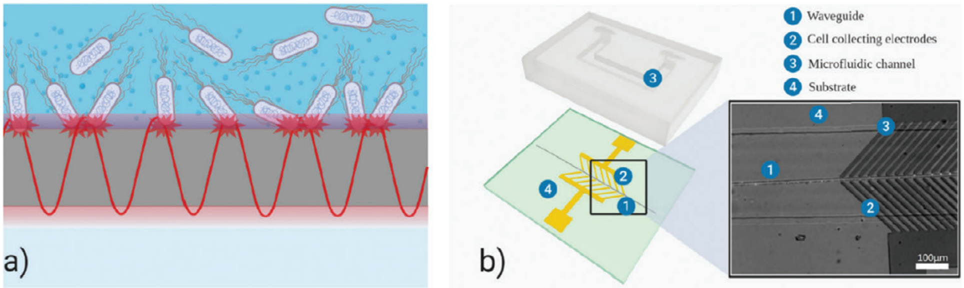

Figure 6. Polymer waveguide with concentrator electrodes for label free detection of E.coli. a) Proof of concept. b) Device construction. Reproduced under the terms of the CC-BY 4.0 license.[48]

∇E^2, which primarily resides on the metal 1 layer, positioned at a notable distance from the sensing waveguide, and is too far to be reached by the evanescent field. Consequently, this spatial separation may lead to analytes not being precisely focused directly onto the sensor surface to be detected. Instead, what may be achieved is a more generalized increase in analyte concentration in the vicinity of the sensor. This is however also a highly desirable effect that will improve sensing sensitivity.

In our second electrode configuration, we opted for a 3D top-bottom layout. Here, one of the electrodes was fabricated on highly doped silicon, seamlessly integrated into the device layer of the PIC. The counter electrode was placed atop a microfluidic channel. This innovative arrangement offers an array of compelling advantages, including the effective mitigation of electroosmotic effects, the creation of highly heterogeneous electric fields, and the potential capability to precisely concentrate analytes within a mere micrometer's distance from the core waveguide surface.

In a related work, a variety of the top-bottom electrode configuration above is described (Figure 5d).[75] Notably, this work focuses on silicon nitride waveguides, distinguishing it from conventional silicon waveguides. This distinction significantly alters the fabrication process and opens up new possibilities for integrating concentrator electrodes.

The substrate (S1) used in fabricating these waveguides consists of a silicon substrate, layered with silicon dioxide and one or more metal layers. These metal layers serve as the foundation for the bottom DEP electrodes. The waveguides are subsequently created through the deposition of silicon nitride, followed by precise etching procedures. To complete the device, a second substrate (S2) is bonded to the first one. This second substrate houses the top electrodes and simultaneously forms the microfluidic channel.

Another recent notable example of a photonic biosensor incorporating DEP for analyte trapping represents the research conducted by Petrowszki et al.[48] In their study, they achieved the detection of E. coli at concentrations on the order of 10^2 CFU/mL using a waveguide sensor platform. As illustrated in **Figure 6** the research team placed gold electrode pairs on a glass cover slip, forming a microscale gap between these electrodes. Within this gap, they fabricated a polymer waveguide designed to efficiently guide light at a wavelength of 670 nm. These electrodes provided the generation of a robust electric field that focused the E. coli bacteria onto the core waveguide. Subsequently, the bacteria could be detected through evanescent-field sensing, utilizing the phenomenon of light scattering. It's noteworthy that although this work does not employ a silicon photonic platform, it serves as a compelling demonstration of successful waveguide evanescent sensing for detecting microorganisms at extremely low concentration levels.

What makes this research particularly intriguing is its clear illustration of how concentrator electrodes can significantly enhance the sensitivity and performance of optical waveguide-based biosensors. This innovative approach showcases the potential of integrating concentration electrodes with photonic waveguides for advanced biosensing applications.

4. Future Prospects

Based on the examples provided, it is evident that only a limited number of electrode or waveguide geometries have been investigated for the implementation of AC electro-kinetics in silicon photonics. Moreover, there is still a need to demonstrate enhanced sensitivity in these sensing platforms. In order to assess the potential of this technology, it is crucial to explore a wider range of photonic waveguides and electrode geometries.

To facilitate the transport of analytes to the sensor surface, it is advisable to position the electrodes on the device layer, either in a coplanar electrode configuration or a top-bottom electrode configuration. For this purpose, highly doped silicon structures on the device layer appear to be the most logical choice, offering a wide range of electrode design possibilities. For increased conductivity of electrode structures, a variety of silicides are available. The increase in conductivity comes however at the cost of more susceptibility to corrosion. Additionally, on bare doped silicon surfaces, a 1–2 nm thick oxide layer forms, which serves the dual purpose of protecting against degradation and preventing side reactions such as electrolysis. However, as a drawback, the oxide layer on the bare silicon surfaces may impede the penetration of the electric field, necessitating the application of higher voltages, similar to what is observed in insulating DEP.[32]

Multiple electrode designs for integration into the device layer of a slot waveguide have been previously introduced and are shown in Figures 5 and 6. In **Figure 7**, we depict simulations of the ∇E^2 that we conducted based on these electrode configurations and the material properties shown in **Table 1**. The materials are taken from several databases[76] with the relative permittivity of PBS puffer set to resemblance water with a value of 80.[39,77] As demonstrated in this figure, a significant ∇E^2 near the waveguide is generated with these electrodes that can be employed to

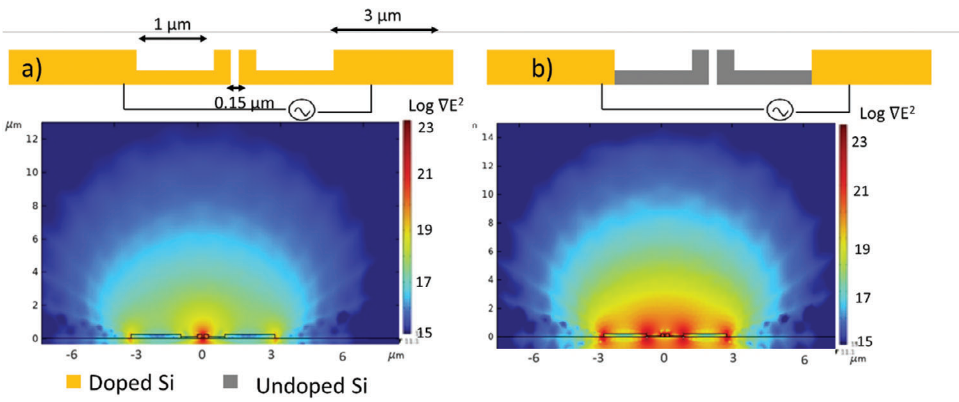

Figure 7. Simulations of electrodes realized on ribbed slot waveguides. a) The entire waveguide is doped to serve as electrodes, with only a short slot separating them at the core waveguide's center. According to FEM simulations using the ACDC module in the software comsol Multiphysics with the parameter shown in Table 1. The highest electric field is generated center of the slot waveguide, which in the figure is placed in the middle b) Simulations with the electrodes farther apart from the core waveguide.

focus analytes with the DEP force. In Figure 7a, the entire waveguide is doped to serve as electrodes, with only a short slot separating them at the core waveguide's center. This configuration produces a maximum at the center of the slot waveguide which is the most sensitive part of the waveguide. While according to simulation the configuration may appear ideal, it also has drawbacks, including modulation of the refractive index in response to the oscillating electric field. Additionally, the close proximity of the electrodes increases the risk of short circuits under strong applied electric fields. Placing the electrodes further apart is a safer option, although issues related to current leakage and modulation may still persist.

For the realization of electrodes on the device layer of other waveguide designs than ribbed slot waveguides, different solutions will be necessary. A promising example is showcased in **Figure 8** with a strip waveguide featuring two electrodes fabricated on the device layer of the SOI wafer. The strongest ∇E^2 is typically observed at the edges of the electrodes; however, there is also a local maximum on the sensor waveguide. Such ∇E^2 distribution has also been reported on similar electrode configurations.[78,79] The local maximum arises in a manner similar to insulating dielectrophoresis (iDEP). In an iDEP setup, insulating structures like posts, membranes, obstacles, or constrictions are incorporated into the microfluidic channel, which deform the applied electric field and create a high electric field gradient with a local maximum within the channel.[80] In the aforementioned electrode structure, the core waveguide acts as an insulating obstacle that generates the local maximum. This effect is highly advantageous for the system as analytes can only be detected approximately within 50–100 nm from the core waveguide.

Table 1. Material properties used in finite element simulations.[76]

Material	Relative Permittivity	Electric Conductivity (S/m)
SiO_2	3.74	10^{-14}
Medium (PBS Puffer)	80	1
Si	11.7	10
n^+-Si	11.7	2×10^4
Metal 1 (aluminum)	1	10^5

The spacing between electrodes plays a pivotal role in determining the strength of the electric field. When electrodes are positioned within a 0.5 µm distance from the core waveguide, the electric field gradient is evenly distributed around it. As the electrodes are moved further apart, the electric field gradient becomes more concentrated at the edges of the electrodes, while weakening near the core waveguide. Nevertheless, maintaining a certain separation between the core waveguide and the electrodes is imperative to prevent evanescent coupling to the electrodes. Therefore, simulations suggest that a spacing of 1–2 µm is often necessary. For slot and rib waveguides, electrodes can be realized in a manner similar to what was described above.

In addition to placing electrodes on the device layer, a second pair of electrodes on the metal 1 layer could be advantageous (Figure 8b). The design of these metal 1-layer electrodes is more flexible compared to those on the device layer, allowing the electric field to penetrate further into the bulk solution. The aim of these electrodes is to capture analytes further away from the waveguide and concentrate them closer to the sensor. These preconcentrated analytes can then more effectively interact with the electrodes on the device layer, designed to transport particles directly onto the core waveguide for detection.

Since the purpose of the metal 1-layer electrodes is not to transport particles directly onto the core waveguide, they can be spaced further apart and wider apart, allowing the electric field gradients to penetrate deeper into the bulk solution (Figure 8c). Furthermore, these metal 1-layer electrodes are typically made of highly conductive materials, which reduces resistance and mitigates the effects of joule heating, particularly at high voltages. The electrodes on the device layer and metal 1 layer can work in tandem, with an AC field applied to the device layer synchronized with an AC field on the metal 1 layer. As illustrated in Figure 8c, this setup generates a strong ∇E^2 maximum at the core sensor surface while also creating a robust field gradient further away from the electrodes, enabling the capture of analytes situated at a distance from the electrodes.

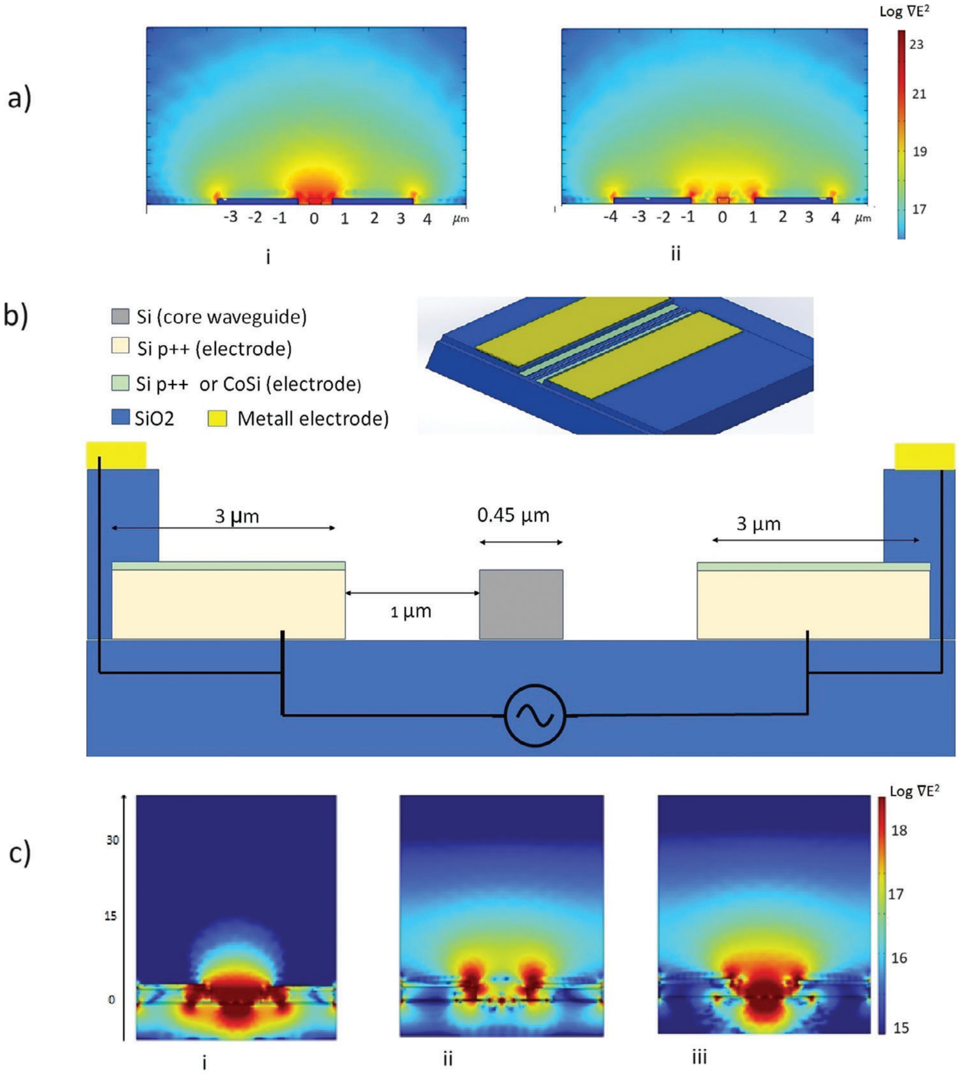

Figure 8. A proposed electrode geometry with a coplanar electrode pair on the device layer next to the sensing waveguide. a) simulated ∇E^2 in (log(∇E^2 /$V^2 m^{-3}$) with the electrodes placed at a distance of i) 0.5 µm and ii) 1 µm from the waveguide. b) cross- section and top view of an electrode pair solution, one placed at the device layer and one at the metal 1-layer. c) Simulated ∇E^2 with i) only the electrodes on the device layer turned on. ii) only the electrodes on the metal 1-layer. iii) electrodes on the device layer and metal 1-layer simultaneously turned on. Reproduced under the terms of the CC-BY 4.0 license.[81]

5. Conclusion

AC electrokinetics is a highly intriguing method that, when combined with biosensors, holds the potential to significantly enhance response times. The development of phase shifters for modulating optical signals in PICs provides a strong foundation for realizing electrodes suitable for AC electrokinetics enhancement of silicon photonic biosensors. These electrodes can be seamlessly incorporated into a PIC through conventional MPW services. Although much of the research aimed at enhancing biosensor responses via AC electrokinetics has remained at the proof-of-principle stage, with integration into PICs currently in a more conceptual phase, it represents a promising field with abundant unexplored avenues for advancing photonic sensing capabilities.

Acknowledgements

The authors acknowledge the support from the German Research Foundation and the Open Access Publication Fund of TU Berlin. This work was funded by the German Federal Ministry of Education and Research (BMBF) within the program "Wissenschaftliches Vorprojekt Photonik" (FKZ 13N15712).

Conflict of Interest

The authors declare no conflict of interest

Author Contributions

A.H. performed conceptualization. A.H. performed methodology. A.H. performed writing—original draft preparation. A.H., P.N., M.B.

writing—review and editing. A.H. performed visualization. A.H. performed project administration. A.H., M.B., and P.N. performed funding acquisition. All authors have read and agreed to the published version of the manuscript.

Keywords

AC electrokinetics, biosensor, dielectrophoresis: electroosmosis, Mach-Zehnder, microring resonator, photonic, PIC fabrication

Received: December 21, 2023
Revised: June 12, 2024
Published online: July 4, 2024

[1] B. Pérez-Fernández, A. de la Escosura-Muñiz, *Anal. Chim. Acta* **2022**, *1212*, 339658.
[2] F. Cros, in (Ed.: R. Narayan), *Biomedical materials*, Springer International Publishing, Cham **2021**, pp. 581–620.
[3] J. Coffel, E. Nuxoll, *Int. J. Pharm.* **2018**, *544*, 335.
[4] C. Chen, J. Wang, *Analyst* **2020**, *145*, 1605.
[5] S. P. Usha, H. Manoharan, R. Deshmukh, R. Álvarez-Diduk, E. Calucho, V. V. R. Sai, A. Merkoçi, *Chem. Soc. Rev.* **2021**, *50*, 13012.
[6] H. Zhu, Z. Fohlerová, J. Pekárek, E. Basova, P. Neužil, *Biosens. Bioelectron.* **2020**, *153*, 112041.
[7] P. Steglich, M. Hülsemann, B. Dietzel, A. Mai, *Molecules* **2019**, *24*, 519.
[8] E. Luan, H. Shoman, D. M. Ratner, K. C. Cheung, L. Chrostowski, *Sensors* **2018**, *18*, 3519.
[9] C. Ciminelli, F. Dell'Olio, D. Conteduca, M. N. Armenise, *IET Optoelectron.* **2019**, *13*, 48.
[10] J. Wang, M. M. Sanchez, Y. Yin, R. Herzer, L. Ma, O. G. Schmidt, *Adv. Mater. Technol.* **2020**, *5*, 1901138.
[11] A. Rahim, J. Goyvaerts, B. Szelag, J.-M. Fedeli, P. Absil, T. Aalto, M. Harjanne, C. Littlejohns, G. Reed, G. Winzer, S. Lischke, L. Zimmermann, D. Knoll, D. Geuzebroek, A. Leinse, M. Geiselmann, M. Zervas, H. Jans, A. Stassen, C. Domínguez, P. Muñoz, D. Domenech, A. L. Giesecke, M. C. Lemme, R. Baets, *IEEE J. Sel. Top. Quantum Electron.* **2019**, *25*, 1.
[12] A. Henriksson, P. Neubauer, M. Birkholz, *Adv. Mater. Interfaces* **2021**, *8*, 2100927.
[13] T. Leitner, G. Friedbacher, T. Vallant, H. Brunner, U. Mayer, H. Hoffmann, *Microchim. Acta* **2000**, *133*, 331.
[14] L. S. Puumala, S. M. Grist, J. M. Morales, J. R. Bickford, L. Chrostowski, S. Shekhar, K. C. Cheung, *Biosensors* **2023**, *13*, 53.
[15] T. M. Squires, R. J. Messinger, S. R. Manalis, *Nat Biotech* **2008**, *26*, 417.
[16] I. Jokić, Z. Djurić, K. Radulović, M. Frantlović, G. V Milovanović, P. M. Krstajić, *Biosensors* **2021**, *11*, 194.
[17] H. Zhang, Y. Qiu, F. Osawa, M. Itabashi, N. Ohshima, T. Kajisa, T. Sakata, T. Izumi, H. Sone, *ACS Appl. Mater. Interfaces* **2023**, *15*, 19892.
[18] N. S. Lynn, J.-I. Martínez-López, M. Bocková, P. Adam, V. Coello, H. R. Siller, J. Homola, *Biosens. Bioelectron.* **2014**, *54*, 506.
[19] C.-C. Chang, L.-M. Fu, R.-J. Yang, in (Ed.: D. Li), Encyclopedia of microfluidics and nanofluidics, Springer US, Boston, MA **2008**, pp. 33–38.
[20] P. Modarres, M. Tabrizian, *Microsyst. Nanoeng.* **2020**, *6*, 60.
[21] S. Sachs, M. Baloochi, C. Cierpka, J. König, *Lab Chip* **2022**, *22*, 2011.
[22] E.-M. Laux, F. F. Bier, R. Hölzel, *Bioelectrochemistry* **2018**, *120*, 76.
[23] A. Salari, M. Thompson, *Sens Actuators B Chem.* **2018**, *255*, 3601.
[24] R. E. Fernandez, A. Rohani, V. Farmehini, N. S. Swami, *Anal. Chim. Acta* **2017**, *966*, 11.
[25] S. Li, H. Cui, Q. Yuan, J. Wu, A. Wadhwa, S. Eda, H. Jiang, *Biosens. Bioelectron.* **2014**, *51*, 437.
[26] A. Henriksson, L. Kasper, M. Jäger, P. Neubauer, M. Birkholz, *Micromachines* **2020**, *11*, 954.
[27] S. Chakraborty, in (Ed: D. Li), Encyclpedia of microfluidics and nanofluidics, Springer US, Boston, MA **2008**, pp. 595–599.
[28] R. Pethig, *J. Electrochem. Soc.* **2016**, *164*, B3049.
[29] A. Henriksson, P. Neubauer, M. Birkholz, *Biosensors* **2022**, *12*, 784.
[30] G. Gonella, E. H. G. Backus, Y. Nagata, D. J. Bonthuis, P. Loche, A. Schlaich, R. R. Netz, A. Kühnle, I. T. McCrum, M. T. M. Koper, M. Wolf, B. Winter, G. Meijer, R. K. Campen, M. Bonn, *Nat. Rev. Chem.* **2021**, *5*, 466.
[31] A. Salari, M. Navi, T. Lijnse, C. Dalton, *Micromachines* **2019**, *10*, 762.
[32] V. H. Perez-Gonzalez, *Electrophoresis* **2021**, *42*, 2445.
[33] Y. Song, P. Chen, M. T. Chung, R. Nidetz, Y. Park, Z. Liu, W. McHugh, T. T. Cornell, J. Fu, K. Kurabayashi, *Nano Lett.* **2017**, *17*, 2374.
[34] J. P. Urbanski, T. Thorsen, J. A. Levitan, M. Z. Bazant, *Appl. Phys. Lett.* **2006**, *89*, 143508.
[35] K. Yoshida, T. Sato, S. I. Eom, J. Kim, S. Yokota, *Sensors Actuators A Phys.* **2017**, *265*, 152.
[36] M. Wu, Y. Gao, A. Ghaznavi, W. Zhao, J. Xu, *Sens Actuators B Chem.* **2022**, *359*, 131611.
[37] M. A. Hayes, A. G. Ewing, *Anal. Chem.* **1992**, *64*, 512.
[38] J.-R. Gong, *Small* **2010**, *6*, 967.
[39] M. E. P. Emmerich, A.-S. Sinnigen, P. Neubauer, M. Birkholz, *Biomed. Microdevices* **2022**, *24*, 30.
[40] S.-I. Han, H. S. Kim, K.-H. Han, A. Han, *Lab Chip* **2019**, *19*, 4128.
[41] V. Abt, F. Gringel, A. Han, P. Neubauer, M. Birkholz, *Microorganisms* **2020**, *8*, 540.
[42] H. Matbaechi Ettehad, P. Soltani Zarrin, R. Hölzel, C. Wenger, *Micromachines* **2020**, *11*, 501.
[43] S. Stanke, C. Wenger, F. F. Bier, R. Hölzel, *Electrophoresis* **2022**, *43*, 1309.
[44] S. A. Muhsin, M. Al-Amidie, Z. Shen, Z. Mlaji, J. Liu, A. Abdullah, M. El-Dweik, S. Zhang, M. Almasri, *Biosens. Bioelectron.* **2022**, *203*, 113993.
[45] A. Atajanov, A. Zhbanov, S. Yang, *Micro Nano Syst. Lett.* **2018**, *6*, 2.
[46] C.-H. Han, S. Y. Woo, J. Bhardwaj, A. Sharma, J. Jang, *Sci. Rep.* **2018**, *8*, 14942.
[47] J. Cottet, O. Fabregue, C. Berger, F. Buret, P. Renaud, M. Frénéa-Robin, *Biophys. J.* **2019**, *116*, 12.
[48] D. Petrovszki, S. Valkai, E. Gora, M. Tanner, A. Bányai, P. Fürjes, A. Dér, *Microelectron. Eng.* **2021**, *239–240*, 111523.
[49] P. Modarres, M. Tabrizian, *Sens Actuators B Chem.* **2017**, *252*, 391.
[50] R. Hölzel, R. Pethig, *Micromachines* **2020**, *11*, 533.
[51] Y. Liu, M. A. Hayes, *Anal. Chem.* **2021**, *93*, 1352.
[52] M. Washizu, S. Suzuki, O. Kurosawa, T. Nishizaka, T. Shinohara, *IEEE Trans Ind Appl* **1994**, *30*, 835.
[53] N. L. Kazanskiy, S. N. Khonina, M. A. Butt, *Micromachines* **2023**, *14*, 1080.
[54] W. Bogaerts, P. De Heyn, T. Van Vaerenbergh, K. De Vos, S. Kumar Selvaraja, T. Claes, P. Dumon, P. Bienstman, D. Van Thourhout, R. Baets, *Laser Photon. Rev.* **2012**, *6*, 47.
[55] H. Niu, P. Yu, Y. Zhu, Z. Jing, P. Li, B. Wang, C. Ma, J. Wang, J. Wu, A. O. Govorov, A. Neogi, Z. M. Wang, *Opt. Express* **2022**, *30*, 29665.
[56] K. J. Freedman, L. M. Otto, A. P. Ivanov, A. Barik, S.-H. Oh, J. B. Edel, *Nat. Commun.* **2016**, *7*, 10217.
[57] C. T. Ertsgaard, M. Kim, J. Choi, S.-H. Oh, *Nat. Commun.* **2023**, *14*, 103.
[58] *2020 IPSR-I Integrated Photonic Systems Roadmap International Chapters*, IPSR-I I **2020**.
[59] S. Y. Siew, B. Li, F. Gao, H. Y. Zheng, W. Zhang, P. Guo, S. W. Xie, A. Song, B. Dong, L. W. Luo, C. Li, X. Luo, G.-Q. Lo, *J. Light. Technol.* **2021**, *39*, 4374.

[60] S. Lischke, A. Peczek, J. S. Morgan, K. Sun, D. Steckler, Y. Yamamoto, F. Korndörfer, C. Mai, S. Marschmeyer, M. Fraschke, A. Krüger, A. Beling, L. Zimmermann, *Nat. Photonics* **2021**, *15*, 925.
[61] A. Rahim, A. Hermans, B. Wohlfeil, D. Petousi, B. Kuyken, D. Van Thourhout, R. G. Baets, *Adv. Photonics* **2021**, *3*, 24003.
[62] M. Birkholz, A. Mai, C. Wenger, C. Meliani, R. Scholz, *Wiley Interdiscip Rev Nanomed Nanobiotechnol* **2016**, *8*, 355.
[63] M. Birkholz, K.-E. Ehwald, P. Kulse, J. Drews, M. Fröhlich, U. Haak, M. Kaynak, E. Matthus, K. Schulz, D. Wolansky, *Adv. Funct. Mater.* **2011**, *21*, 1652.
[64] I. Krylov, Y. Qi, V. Korchnoy, K. Weinfeld, M. Eizenberg, E. Yalon, *J Vac Sci Technol A* **2020**, *38*, 32403.
[65] H. Zheng, R. Zhang, Q. Xu, X. Kong, W. Sun, Y. Fu, M. Wu, K. Liu, *Materials (Basel)* **2023**, *16*, 622.
[66] M. Jacques, A. Samani, E. El-Fiky, D. Patel, Z. Xing, D. V Plant, *Opt. Express* **2019**, *27*, 10456.
[67] G. T. Reed, G. Mashanovich, F. Y. Gardes, D. J. Thomson, *Nat. Photonics* **2010**, *4*, 518.
[68] J. Mulcahy, F. H. Peters, X. Dai, *Photonics* **2022**, *9*, 40.
[69] H. Sun, Q. Qiao, Q. Guan, G. Zhou, *Micromachines* **2022**, *13*, 1509.
[70] M. Jäger, J. Bruns, E. Ehrentreich-Förster, K. Petermann, in *Adv. Photonics 2013* (Ed: M. K. Ewing), Optica Publishing Group, Rio Grande, Puerto Rico **2013**, p. ST4B.3.
[71] K. F. Erik Enebakk, Jan-Ove Odden, in *Proc. Silicon Chem. Sol. Ind.* **2022**.
[72] C.-I. Tsai, P.-H. Yeh, C.-Y. Wang, H.-W. Wu, U.-S. Chen, M.-Y. Lu, W.-W. Wu, L.-J. Chen, Z.-L. Wang, *Cryst. Growth Des.* **2009**, *9*, 4514.
[73] B. Tsuyoushi, Fine Particle Sensing Element and Fine Particle Evaluation System **2018**, JP2018031593A.
[74] P. Moock, L. Kasper, M. Jäger, D. Stolarek, H. Richter, J. Bruns, K. Petermann, *Opt. Express* **2018**, *26*, 22356.
[75] D. Carothers, Waveguide Enhanced Analyte Detection Apparatusle **2021**, CA3175327A1.
[76] T. C. Edwards, M. Steer, in *Found. Microstrip Circuit Des*, Wiley-VCH Verlag, Weinheim **2016**, pp. 635.
[77] A. Salmanzadeh, M. B. Sano, R. C. Gallo-Villanueva, P. C. Roberts, E. M. Schmelz, R. V Davalos, *Biomicrofluidics* **2013**, *7*, 11809.
[78] H. J. Kim, H. Ahn, D. S. Lee, D. Park, J. H. Kim, J. Kim, D. S. Yoon, K. S. Hwang, *Sensors* **2019**, *19*, 4152.
[79] V. V Kostyuchenko, E. G. Zaytseva, O. V Naumova, in 2023 IEEE 24th Int. Conf. Young Prof. Electron Devices Mater **2023**, pp. 1410.
[80] B. H. Lapizco-Encinas, *Electrophoresis* **2019**, *40*, 358.
[81] A. Henriksson, P. Neubauer, M. Birkholz, *Design and Simulation of Si-Photonic Nanowire-Waveguides with DEP Concentration Electrodes for Biosensing Applications*, **2024**, arXiv:2406.19534

Anders Henriksson earned a master's degree in organic chemistry at Linköping University. He continued with doctoral studies in applied surface chemistry at the Vienna Technical University under the supervision of Prof. Helmuth Hoffmann and subsequently spent one year as a JSPS research fellow at Tokyo University in the Nishihara lab. Since 2017 he is working at TU Berlin as a post doc in the joint lab bioelectronics TU Berlin/IHP and his research is focusing on combining dielectrophoresis with photonic biosensors.

Peter Neubauer is Professor of Bioprocess Engineering at the Department of Biotechnology at the Technische Universität Berlin, Germany, since 2008. He holds a doctoral degree in Microbiology from Universität Greifswald, Germany, and completed postdocs at the Royal Institute of Technology (KTH), Sweden, and Martin-Luther-Universität of Halle-Wittenberg, Germany, before he received a professorship in Bioprocess Engineering from the University of Oulu, Finland (2000–2008). His research is concerned with bioprocess scale-up/scale-down and microbial physiology in industrial scale bioprocesses, bioprocess analytical technologies and mathematical modeling of bioprocesses.

Mario Birkholz is Professor for Bioelectronics at TU Berlin and Head of the Joint Lab Bioelectronics formed between TUB and IHP, the Leibniz-Institut für innovative Mikroelektronik in Frankfurt (Oder). He is a physicist by education and did his first research in biophysics at the FU Berlin before completing his PhD on semiconducting materials for photovoltaics at Hahn-Meitner-Institut Berlin, now Helmholtz-Zentrum für Materialien und Energie. As a postdoc at Fraunhofer IST in Braunschweig, his research focused on thin films, their structure and morphology, and their shaping by growth processes. He is known to some readers as author of the textbook "Thin Film Analysis by X-ray Scattering".